EURASIP Journal on Wireless Communications and Networking

RESEARCH Open Access

A dynamic handover scheme based on bidirectional VLC channel in multi-user attocell networks

Liqiang Wang[1], Dahai Han[1*], Min Zhang[1], Jingtao Wu[1], Xiaotian Jiang[1] and Jingsuo He[2]

*Correspondence: dahaihan@foxmail.com

[1] State Key Laboratory of Information Photonics and Optical Communications, Beijing University of Posts and Telecommunications, Beijing 100876, China
[2] Physics Department, Capital Normal University, Beijing 100048, China

Abstract

Light fidelity (LiFi) would be a potential optical wireless communications technology for future mixed-spectrum 5G/6G indoor attocell network, which uses light-emitting diodes based as an optical antenna and offers Gbits capacity. For this scenario, a dynamic handover scheme based on bidirectional visible light communications (VLC) channel is proposed, which uses the uplink light sources to characterize terminal's movement status for the mobility and make the handover decision in contrast to the unidirectional links. The uplink reference signal received power and the movement state are examined, and the created algorithm is executed in the bidirectional VLC test bed. The experimental results show that the proposed method will reduce the terminal's handover rate by up to 45% and increase the optical network throughput by up to 26% at the experimental data rate compared with the skipping handover scheme for indoor LiFi network.

Keywords: Light fidelity (LiFi) attocell, Visible light communications (VLC), Handover, Bidirectional, Reference signal received power (RSRP)

1 Introduction

With the rapid development of wireless digital devices and the growing expansion of the Internet of things (IoT), expanding or efficiently using frequency spectrum resources has become an important means to cope with the increasing wireless traffic [1]. To deal with the exponentially growth in data usage, 5G wireless networks and beyond will also explore new advanced and complementary technologies of millimeter wave, massive multiple input multiple output and optical wireless [2]. The optical wireless communication (OWC) covers the ultra-volte, infrared (IR), blue-green light and visible bands offering bandwidth orders of magnitude higher than the radio frequency (RF) frequencies, where the later better known as the visible light communications (VLC) have received a great deal of attention within the contest of 5G and beyond [3–6]. Note that VLC as a disruptive key technology is also included in the 6G network [7].

Within the context of broadband 5G/6G, light fidelity (LiFi), which has optical specific characteristics in contrast to the wireless communications, is envisaged to provide speeds 100 times faster than WiFi over a short transmission range by simply using the

light-emitting diode-based lighting fixtures. In addition, the deployment of LiFi-based attocell access point (AP) which broadcasts data in the downlink channel and allocates a fixed time slot for each terminal in the uplink channel by time division multiple access (TDMA) mechanism will (i) enhance wireless data capacity for IoT and 6G; (ii) overcome the transmission blind spots in indoor environments; and (iii) meet multi-terminal connectivity and the cross-cell handover for the mobile terminals. Note that a use case for a bidirectional LiFi attocell network is shown in Fig. 1a. However, in LiFi network there are challenges including the backhaul of hundreds of base stations and frequent handovers since the APs usually have a much small coverage area [8], thus the need for fast and efficient handover strategy and the terminal's movement estimation as well.

Deployment of small BSs will increase throughput, but also increase handover rate R_{ho}, the signaling overhead and the interference level in RF [9]. However, due to the high throughput requirements and the limitations of LEDs power and the field of view (FoV), the dense deployment of attocells is an efficient solution. In the traditional handover strategy, the reference signal received power (RSRP) is a simple and popular indicator for handover decision-making; RSRP level of the adjacent AP is monitored against the currently accessed AP for immediate switching. However, with no protection mechanism, the link may experience multiple handovers due to a single decision criterion, which will result in an additional signaling overhead and increased latency, thus eventually leading to the ping-pong effect and ultimately degraded the quality of services (QoS) as well as link failures. In [10], an improved traditional handover strategy, which delays handover by adding a static window period, was proposed, effectively deducing the ping-pong effect. In [11, 12], handover skipping method was investigated to effectively mitigate frequent handover, which is compatible with RF-based cellular networks, whereas in [13], a method based on the terminal's movement trajectory was introduced, which adopted a new mathematical method to enhance the QoS for service providers. However, in [13] only a VLC link was used in the downlink for handover, and no uplinks

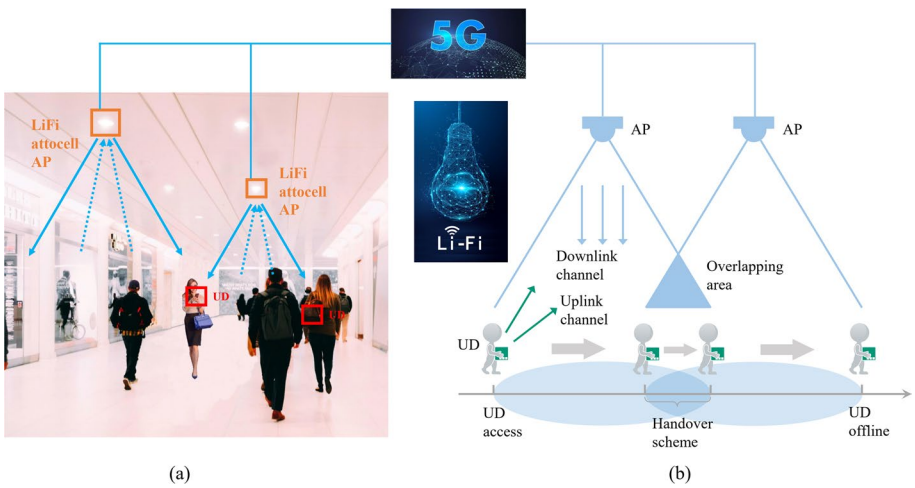

Fig. 1 **a** A use case of a bidirectional LiFi attocell network and **b** the LiFi attocell system block diagram. In figure, where it is illustrated in "Introduction" section, **a** depicts application scenario of a bidirectional light fidelity attocell network, **b** shows a communication demo and the scope to which the handover process occurs

(VLC or RF) were employed to upload a larger amount of terminal information quickly and efficiently. In [14], a smart handover management scheme based on topology aware handover skipping with terminal trajectory estimation in single- and two-tier downlink networks was investigated with a 47% gain in the average throughput. Note that the already mature handover strategies used in RF wireless communication systems cannot simply be adopted in VLC system due to different frequency spectrum bands and channel characteristics.

Currently, researchers prefer to use vertical handover method in heterogeneous VLC network, because of no decision being made on the use of wireless technology (VLC, IR, WiFi and RF) for the uplink. This paper is working on the optical link handover method for multiple LiFi terminals connecting to LiFi APs. As illustrated in Fig. 1b, the bidirectional VLC link unifies the up- and downlink channels, which greatly helps to reduce the complexity and cost associated with channel diversification.

In this paper, we propose an efficient and flexible optical handover strategy that refers the VLC uplink status in the bidirectional indoor LiFi network. The proposed scheme utilizes the uplink's RSRP (uRSRP) to help algorithmic decision-making and efficient handover, where it assesses the user device (UD) movement and its direction by detecting the changes in the uRSRP level. R_{ho}, which is equal to the UD's speed divided by the average path length and reflects the speed of the handover, average throughput and accessibility probability are evaluated to achieve a balance between the handover costs and the QoS. Different from research on the impact of orientation of UD as receiver in downlink on system performance such as throughput and delay as in [15–18], we just use the directivity of visible light in uplink to assist the decision of the handover algorithm, which hardly affects the system performance in downlink; therefore, in this paper, the orientation will not be analyzed in detail here. Moreover, different from the traditional trajectory-based and handover skipping methods as in [11, 12], in the proposed handover strategy there is no need to record much movement of the mobile terminal in order to make predictions about its future states. In addition, it is much more flexible than handover skipping and therefore more scenarios can be considered.

A bidirectional VLC system model is proposed in Sect. 2 based on the random waypoint (RWP) model, which can fully correlate the RSRP according to the terminal's distance to the adjacent optical antenna. In Sect. 3, the optical terminal handover scheme is described. The mathematical expressions are derived, and the performance of the proposed scheme in terms of R_{ho} and accessibility probability are analyzed theoretically in Sect. 4. The results obtained from the OMNeT++ platform and a hardware experimental platform are demonstrated in Sect. 5. Section 4 concludes related works on handover costs and system QoS.

2 System model

We considered an indoor VLC system, where its system model is illustrated in Fig. 2 which is composed of APs including Txs and Rxs (i.e., photodiodes) and UD. Each AP has a constant and identical circular luminance area projected on the floor level with a given field of view. The overlap region between APs $s_{i,j}$ is selected as $s_{i,j} = (\pi - 2) \bullet r^2/8$ based on the principle that the overlap region is covered by at most two AP's valid signal areas, where i and j represent specific AP and r is the

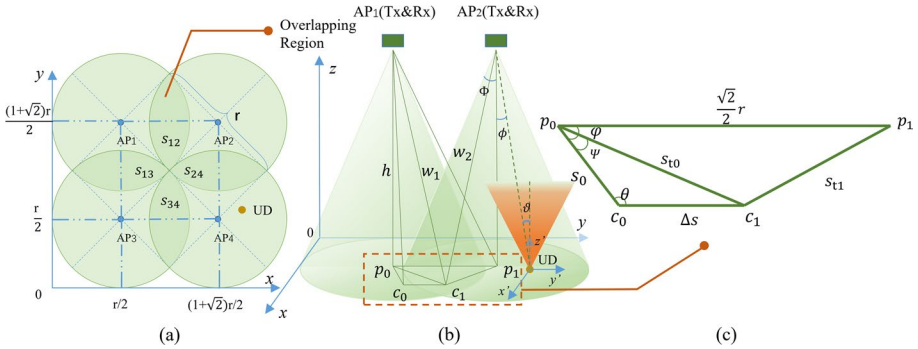

Fig. 2 Relevant diagram of system model: **a** A distribution mode of APs, **b** an AM model and **c** a geometry diagram of the AM model projected on the ground. Figure is illustrated in "System model" section. **a** shows a top view of four access points coverage and their geometric annotations. **b** depicts the access model in bidirectional visible light communications system, the light green and orange part illustrate the coverage of visible light signal from access point in downlink and from user' terminal in uplink, respectively. **c** illustrates the geometric structure projected on the ground from **b**

diameter of the effective coverage region of a single AP. Note that the up- and downlink employ different spectra without causing conflict; therefore, the bidirectional VLC system can actually realize full-duplex communication. Besides, we consider the impact of minimizing the normal lighting functions and the general lighting node distribution logic, so that APs are uniformly distributed with sufficient and regular overlap of the coverage area.

The access mobility (AM) model, which is based on the RWP model commonly used in wireless cellular communications, is adopted in this work; see Fig. 2b [19]. p_0 and p_1 are the center of illumination area for the APs 1 and 2, respectively, and w_1 and w_2 are the distance between the UD and APs, respectively. Φ represents the FoV of the Rx, ϕ and ϑ denote the angles of transmitter and incidence. Note that (i) the UD will initiate a handover process in the overlapping regions $s_{i,j}$; and (ii) no limitation on the movement of the UD and the model works in most cases. Figure 2c illustrates a geometry diagram of the AM model projected on the ground.

The initial position of UD is denoted by c_0, and c_1 is the current position in the overlapping area (OA). The UD distances at time t_0 from p_0 and p_1 are given as, respectively:

$$s_{t_0} = \sqrt{s_0^2 + \Delta s^2 - 2 s_0 \Delta s \cos\theta}, \tag{1}$$

$$s_{t_1} = \sqrt{s_{t_0}^2 + \frac{r^2}{2} - \sqrt{2} r s_{t_0} \cos(\varphi - \psi)}, \tag{2}$$

where s_0 is the initial UD distance from the AP's center, Δs is the distance between the current and initial UD positions; and $\theta = \pi - \arccos\left(\frac{\overrightarrow{p_0c_0} \bullet \overrightarrow{c_0c_1}}{|p_0c_0||c_0c_1|}\right)$. Ψ denotes the movement angle of UD relative to p_0, i.e., UD's positions at t_0 and t_i, which is given as

$$\psi = \arcsin \frac{\sin\theta \cdot \Delta s}{s_{t_0}}. \tag{3}$$

The distance w_i between the UD and AP_1 and AP_2 at time t_0 is given, respectively, as

$$w_1 = \sqrt{h^2 + s_{t_0}^2}, \tag{4}$$

$$w_2 = \sqrt{h^2 + s_{t_1}^2}, \tag{5}$$

where h is the height of APs from the ground level.

3 Movement estimation and handover scheme

The handover process is designed to ensure the UD's mobility and access to the best serving AP for high QoS. Monitoring the average received signal strength level is one option to determine the best serving AP. For selecting the best serving AP, there are a number of criteria including latency, data throughput and load balancing [20]. Note that the handover cost and complexity are always increasing functions of the AP's density. In our proposal, we have used RSRP, which comprises the signals received by a UD from APs and by a photodiode (PD) from UDs. Note that knowledge on the UD's direction of movement is critical in the handover process. Figure 3 shows the UD movement path covering a number of cells.

The RSRP responses to the PDs in different directions represent the UD's movement direction at that moment. PDs are used to detect uRSRP and receive the location information from UDs continuously in the upstream, which is connected to the current AP. Here, we consider three movement scenarios for evaluating the proposed algorithm:

Path 1: The UD moves straight from one cell to another by crossing a single OA. uRSRP keeps increasing until it is higher than the threshold, thus initiating the handover. In this scenario, the handover process can be completed much faster while maintaining

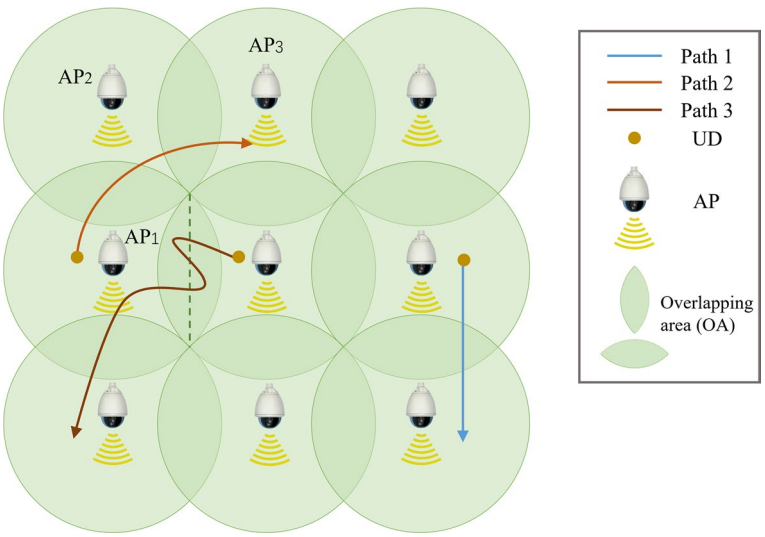

Fig. 3 Diagram of UD's movement path. Figure shows three typical movement paths of users under coverage of access points. Blue, orange and brown lines represent the type of user movement where immediate handover, handover skipping and complex handover condition may occur, respectively

the connectivity for the UD with reduced load on the handover decision process, thus no need for a handover process that requires complex calculations.

Path 2: The UD moves from AP_1 to AP_3 via AP_2, thus crossing two OAs. We set up a first-in-first-out (FIFO) cache mechanism, where resource blocks are queued in the cache of APs while channel fluctuating is at the edge of APs or the shadow regions with blocking. Note that the blockage of the light path caused by the obstacle or the change of the UD's movement orientation may be a potential influence on the UD's QoS. [8] shows that the blockage has little impact on the handover rate in handover schemes with no protection mechanism, while UD's speed is 5 m/s. Therefore, the FIFO cache mechanism could almost eliminate the impact on UD's connectivity and QoS caused by the brief light path blockage. In the case of a downlink channel being blocked due to human activities, etc., or a handover occurs before a packet completes the transmission, the packet will be retransmitted. In cases where continuous high throughput in optical network is more important, the AP should be switched immediately during the optical link blocking; however, we are more focused on the impact of handover cost; therefore, we set the dwell time window $\mathcal{TW}$ in order to ensure continuous data transmission and maintain the original link as much as possible. If the link blocking is not restored when $\mathcal{TW}$ expires, the UD will switch to the AP for SNR_{max}. In addition, in multi-terminal environments the links are affected by higher level of interference (co- and adjacent channel); therefore, for the UD we consider the signal-to-noise ratio (SNR) in an additive white Gaussian noise channel. Note that, in handing over UD from AP_1 to AP_3 via AP_2 the SNR from only AP_2 or both AP_2 and AP_3 are monitored and the handover is completed until the SNR_{max} for AP_3 is detected. When the UD moves to the area of AP_2 and the SNR values of AP_1 and AP_3 are low (i.e., no connection), the UD should continue to read packets from the FIFO cache within $\mathcal{TW}$ to ensure uninterrupted communications with the maintained QoS. If the SNR due to AP_2 is at its maximum at time greater than the period of the $\mathcal{TW}$ (i.e., $t_{\mathcal{TW}}$), then the UD is switched to AP_2. Therefore, this handover method is not only applicable to the above scenario where a UD briefly passes through the coverage area of an adjacent AP, but also applies to the scenario where a UD moves so fast that it stays in the coverage area of an AP for too short a time.

Path 3—The UD back-and-forth movement trajectory and direction may be constantly changing within the OA, thus resulting in a ping-pong effect where $\mathcal{TW}$ is refreshed continuously while the original connection is still maintained.

The judgment of the direction of a UD's movement is the premise of the handover decision for the algorithm implement. Therefore, we can obtain the direction of a UD's movement near this moment by taking the maximum value of u_i that represents i^{th} PD and receives uRSRP from a UD. Since APs are evenly distributed in indoor environment, and we considered three typical modes of a UD's movement that can cover most situations in the handover scheme. Therefore, the direction of a UD's movement should be divided into positive direction D and diagonal direction X relative to the room for executing the algorithm. When the direction of a UD's movement is positive and satisfies the scenario of Path 1, it only needs to judge $\max\{d_{connected}, d_{candidate}\}$ that the UD can switch to the target AP if its SNR is greater than that of the current AP. When the direction of a UD's movement is diagonal direction, taking Path 2 as an example, it is necessary to determine whether the UD needs to carry out a skipping handover scheme

in combination with the accessibility probability. When a UD is in Path 3, the dwell time window will be set to infinity to maintain the UD's original connection. The pseudocode of the optical handover method is illustrated in Algorithm 1.

Algorithm 1 Proposed handover algorithm

Input: positive direction D, diagonal direction X;
Output: action h_{or};
  while $t < t_{TW}$ do
    for each $i \in$ n, do
      d(i) = argmax$\{u_i\}$;
      if d(i) $\in D$ then
        $h_{or} \Longleftarrow \max\{d_{connected}, d_{candidate}\}$;
      else if d(i) $\in X$ then
        $h_{or} \Longleftarrow (d+u_i^{-\lambda})/(d+1+10^{\gamma/10})$;
      else
        t_{TW} = inf;
        $h_{or} \Longleftarrow 0$;
    end for
  end while

Since the UD's mobile state is randomly and dynamically changing, the algorithm should adapt itself to hand over decisions for different mobile situations.

4 Theoretical analysis

We assume that APs and PDs are uniformly distributed in the room, as shown in Fig. 2b, and there are several UDs wondering in varied routes in Fig. 3. In the case of multi-terminal, the clock signal will drift, which would lead to the optical phase shift, thus resulting in bit errors. In practice, ambient noise differences and third-party terminal interference could result in link status deterioration [21]; here, we consider the ideal condition. We have made a number of assumptions including not considering the impact of NLoS, higher SNR, employing high-pass filter, and frame or bit synchronization. We use the SNR for UD handover from 1 to N, which is positively related to the downlink RSRP (dRSRP) for making a decision on which AP is more likely to serve the UD. The handover is carried out when SNR > γ, where SNR is from the target AP that is selected as the UD's movement and γ denotes the threshold level. In order to ensure connectivity, the UD will select an AP corresponding to the $\text{SNR}_{\max}$ even though SNR < γ. The SNR of the UD can be expressed as

$$\text{SNR} = \frac{\left(P_{\text{tr}} h_c R_{\text{pd}}\right)^2}{N^{LiFi} B^{LiFi}}, \tag{6}$$

where P_{tr} represents the AP's transmit power, the detector response is represented by R_{pd}, N^{LiFi} is the power spectral density (PSD) of noise at the UD detector, B^{LiFi} is the bandwidth of a LiFi AP, the channel gain is denoted by h_c, which is given by [22]:

$$h_c = \frac{(m+1)A_{da}}{2\pi w_i^2} \cos^m \phi g_s(\vartheta) g(\vartheta) \cos\vartheta, \tag{7}$$

where Lambertian radiant order is denoted by $m = -\ln 2/\ln\cos\Phi_{1/2}$, A_{da} represents the detector area of the UD, and $g_s(\vartheta)$ and $g(\vartheta)$ are the optical signal transmission filter and the optical concentrator gain, respectively.

4.1 Optical handover rate

We present the UD's average moving distance which is denoted by $\overline{d}_{\mathrm{path}}$ in a square area (see Fig. 2), where handover may occur. Assuming that a and b are random points in the edge of a square region with the side length r, a and b follow a uniform distribution with the probability density function given:

$$p(a) = p(b) = \frac{1}{r}. \tag{8}$$

The distribution function of a square for a line segment length projected to the x-axis in the region can be expressed as

$$\begin{aligned} F(x) &= P(X \le x) = P(T^2 \le x) \\ &= \int_0^{\sqrt{x}} f(t)\mathrm{d}t = \frac{2}{r^2}(\sqrt{x} - \frac{x}{2}), \end{aligned} \tag{9}$$

where T is the random variable of t in the distribution function, and $f(t)$ is the probability density function with the distribution function, which is given as

$$\begin{aligned} F(t) &= \iint\limits_{(a-b)^2 \le t^2} p(a)p(b)\mathrm{d}a\mathrm{d}b \\ &= \iint\limits_{-t \le |a-b| \le t} \frac{1}{r^2}\mathrm{d}a\mathrm{d}b\, a, b \in [0, r] \\ &= \frac{1}{r^2}(2t - t^2). \end{aligned} \tag{10}$$

The length obtained by Pythagorean theorem is denoted as $Z = X + Y$; therefore, the distribution function is given as

$$\begin{aligned} F_Z(z) &= P\{Z \le z\} = P\{X + Y \le z\} \\ &= \iint\limits_{D_z} f(x, y)\mathrm{d}x\mathrm{d}y, \end{aligned} \tag{11}$$

where

$$D_z = \{(x, y) | x + y \le z\}. \tag{12}$$

The probability density function of z can be expressed as

$$f_Z(z) = \int f(x, z - x)\mathrm{d}x, \tag{13}$$

where x and y are independent of each other and with the joint probability density function given as

$$f(x, z-x) = f(x)f(z-x). \tag{14}$$

In a specific region, the probability density function of the square for a line segment length can be computed as

$$g(z) = \begin{cases} \int_0^z f(x)f(z-x)\mathrm{d}x \; 0 \le z < r^2 \\ \int_{z-r^2}^{r^2} f(x)f(z-x)\mathrm{d}x \; r^2 \le z \le 2r^2 \end{cases}, \tag{15}$$

$$\Rightarrow$$

$$g(z) = \begin{cases} \frac{\pi - 4\sqrt{z} + z}{r^4} \; 0 \le z < r^2 \\ \frac{\pi - 4\arctan\sqrt{z-1} + 4\sqrt{z-1} - 2 - z}{r^4} \; r^2 \le z \le 2r^2 \end{cases}, \tag{16}$$

where $z \in [0, 2r^2]$.

Next, we obtain the expectation $\mathbb{E}(l)$, which is given by

$$\overline{d}_{path} = \mathbb{E}(l) = \int_0^{\sqrt{2}r} l \cdot g(l^2) \cdot 2l\mathrm{d}l. \tag{17}$$

Finally, R_{ho} of UD is given by

$$R_{\mathrm{ho}} = \frac{v}{r}\left[\frac{103\sqrt{2} - 74}{45} - \ln(1+\sqrt{2})\right]^{-1}, \tag{18}$$

where v is the UD velocity and $[.]\cdot r$ is the average path length [8].

4.2 Accessibility probability

The accessibility probability of the UD as a function of γ and d is given as

$$\mathcal{P}(\gamma | d; u_i; i = 1, 2...n) = \frac{d + u_i^{-\lambda}}{d + 1 + 10^{\gamma/10}}, \tag{19}$$

where d represents the UD's dRSRP under the current AP connection; u_i is the i^{th} PD, which receives uRSRP from the UD from all directions, i denotes the different directions and λ is the uRSRP impact factor, which represents the decision weight of uRSRP in the handover algorithm.

Figure 4 shows the accessibility probability $\mathcal{P}$ plots as a function of the SNR threshold γ for (a) a range of dRSRP and (b) λ using (19) and parameters shown in Table 1. As shown, $\mathcal{P}$ decreases with increasing γ and λ and decreases with dRSRP. For example, in Fig. 4a at γ of 5 dB $\mathcal{P}$ is increased from 0.49 to 0.65 for dRSRP of 2 and 5, respectively, whereas in Fig. 4b the increase in $\mathcal{P}$ is from 0.43 to 0.65 for λ of 5 and 0.1, respectively. Note that, at lower values of γ the UD with mobility meets the handover

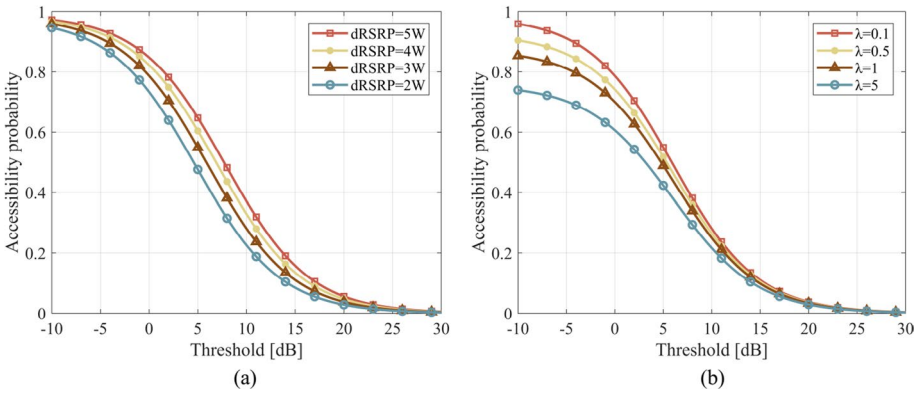

Fig. 4 Accessibility probability versus the threshold for: **a** dRSRP and **b** λ. Figure depicts the relationship of accessibility probability with threshold. **a** shows the change of their relationship in different conditions; red, yellow, brown and blue lines are the cases where downlink reference signal received power is equal to 5 W, 4 W, 3 W and 2 W, respectively. **b** shows the cases of uplink reference signal received power impact factor is equal to 0.1, 0.5, 1 and 5

Table 1 Key simulation parameters

Parameter	Value
Room size (length by width by height)	10 m × 10 m × 3 m
Power spectral density of noise, N^{LiFi}	10^{-21} A^2/Hz
Half-intensity radiation angle,$\Phi_{1/2}$	30°
Dwell time window, $\mathcal{TW}$	0.5 s
Constant variable of system capacity,δ	0.3
Transmission delay, T	0.7 ms
Handover delay,τ	1340 ms
Spectral efficiency, $\mathcal{X}$	1.07 nats/sec/Hz
Diameter of the effective coverage region of a single AP, r	2 m
Detector area of the UD, A_{da}	10^{-4} m^2
Bandwidth per AP, B^{LiFi}	5 Mbps
Downlink RSRP, d	3 Watt
Uplink RSRP, u	2 Watt

conditions, thus leading to increased R_{ho} and latency as well as resulting in the ping-pong effect. Therefore, increasing λ will result in more handover at lower levels of γ.

4.3 Average throughput

We consider an ideal situation where the handover overhead is ignored. The average throughput of the LiFi optical network is given denoted [13]:

$$\mathcal{TP} = B(1-\delta)(1-h_{cost})\mathcal{X}, \tag{20}$$

where B is the overall bandwidth and δ is a constant representing a fraction of the system's capacity [23]. The handover cost h_{cost} is defined as follows [13]:

$$h_{cost} = R_{ho} * \tau, \tag{21}$$

where τ represents the handover delay,

$$h_{\text{cost}} = \frac{v\tau}{r}\left[\frac{103\sqrt{2}-74}{45} - \ln(1+\sqrt{2})\right]^{-1}. \tag{22}$$

In (20), spectral efficiency is defined as follows [14]:

$$\mathcal{X} = \int_0^{\infty} \mathbb{P}\{\log(1+SNR) > x\}\mathrm{d}x, \tag{23}$$

where $\mathbb{P}$ denotes the probability that the inequality in brace is true.

By the change of variables $t = e^x - 1$, spectral efficiency can be rewritten as

$$\mathcal{X} = \int_0^{\infty} \frac{\mathbb{P}\{SNR > t\}}{t+1}\mathrm{d}t. \tag{24}$$

5 Results and discussion

The feasibility of the scheme in terms of latency and the access delay was verified by means of experiments. In addition, the simulation was carried out to evaluate the proposed handover method using the system model developed in OMNeT++. It is assumed that each UD has the same communication conditions within the coverage of each AP. The values of parameters are summarized in Table 1, which are based on experimental data and typical parameters reported for commercially available devices.

The schematic block diagram of the experiment setup is depicted in Fig. 5, which illustrates internal structure and working principle of bidirectional VLC system. A PC (with an Ubuntu OS installed) acts as a server to connect to APs via network cables; the APs transmit and receive VLC data through LED and optical Rx, respectively. On a user side, the user carries out visual operation by holding a PAD (a Surface Pro equipped with Win10 system is used in the experiment), the PAD via a network cable

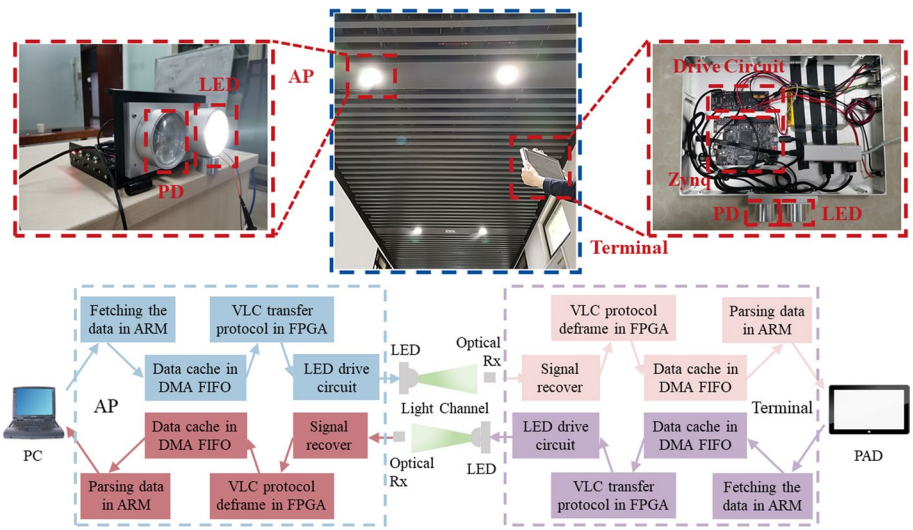

Fig. 5 Block diagram of the experiment setup. The photograph shows the Tx, channel and the Rx. Figure shows internal structure and working principle of the bidirectional VLC system. Blue and pink blocks represent downlink system workflow. Similarly, purple and red blocks represent downlink system workflow

is connected to a terminal that contains LED, optical Rx and some circuit systems to constitute a UD, and the UD communicates with APs via VLC. The protocol code runs on the Zynq-7000 SoC board of both APs and UDs, the data are computed on the ARM, and processing of MAC frames is implemented on the FPGA part of the board. The DMA FIFO is a cache mechanism used to deal with the inconsistent processing speeds between ARM and FPGA. Here, the handover scheme under experiment is the base type, which is to obtain the basic parameter values of the VLC system, independent of the point of innovation. We experimentally measured the handover delay τ_{ho} for 1340 ms and which is adopted in complex simulation environments with higher number of APs and the proposed handover scheme.

5.1 Simulation experiment

For simulation experiments, we have considered 9 APs, which are spaced apart by $\sqrt{2}$ m based on $r=2$ m and uniformly distributed on the ceiling (see Fig. 6a); note that the use of different colors is just to visually distinguish well the coverage area of each AP and has no other meaning. We used the proposed scheme to determine the handover distribution of UDs in VLC network, as shown in Fig. 6b. We counted the handover distribution in the experiment and used the bicubic interpolation to obtain a three-dimensional graph as shown in Fig. 6b, where the probability of handover is significantly increased in the OAs between APs, and therefore it is nearly impossible to switch over in areas covered by a single AP. Note that, in areas where 4 APs intersect, the probability of handover is reduced; this is because handover skipping is more likely to occur in these regions. From Fig. 6b, we observe (i) more handovers in the OA between two adjacent APs; and (ii) lower probabilities of handover closer to the intersection areas of adjacent four APs, which proves that the handover scheme proposed by us that a UD will directly connect to another AP when the UD briefly passes through the coverage area of an adjacent AP and then enters the coverage area of another AP is effectively verified.

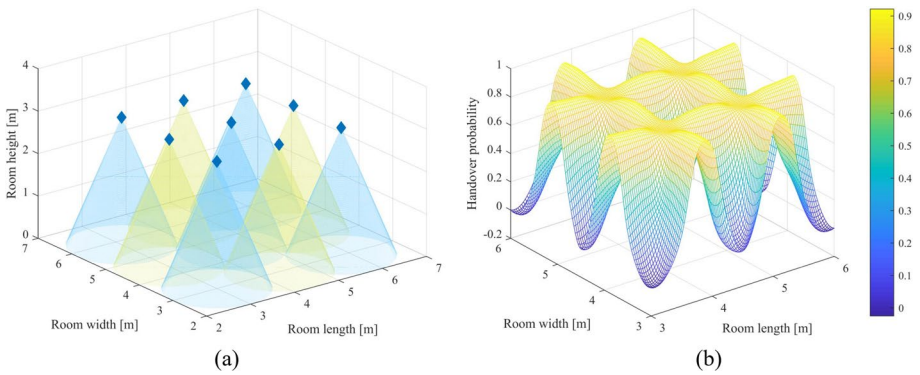

Fig. 6 **a** Indoor distribution of analyzed APs and **b** probability distribution of handover. Figure **b** illustrates the probability distribution of handover where indoor distribution of access points in **a**. The warmer the color, the higher the handover probability in **b**. Different colors are just to visually distinguish well the coverage area of each access point and have no other meaning in **a**

5.2 Results of handover rate

Figure 7 depicts the handover rate R_{ho} versus the rate of closest attocell changing ς for proposed, immediate handover (IHO), dwell handover (DHO) and skipping handover (SHO) schemes. Note that R_{ho} increases with ς in all plots, but at a lower and a higher rate for proposed and IHO schemes, respectively. In the proposed scheme, R_{ho} reaches a maximum level of 0.83 at ς of 2.1 beyond which it reduces. Analysis shows that the rate of closest attocell changing is faster than the normal walking speed. The UD might change its direction of movement in a small area frequently and keep the connection with the original AP as much as possible in order to reduce R_{ho}, thus avoiding the ping-pong effect and maintain the required QoS.

In DHO scheme, $\mathcal{TW} = 0.5$ s in order to avoid the ping-pong effect. For comparison, we have adopted the same value. For the proposed scheme with $\varsigma = 1.5\text{s}^{-1}$, R_{ho} is reduced by 61, 45 and 13% at least compared with IHO, DHO and SHO methods, respectively, while ς increases to 2.5s^{-1}, corresponding to the decrease in R_{ho} by 73, 60 and 45% compared with IHO, DHO and SHO, respectively.

5.3 Results of average throughput

We divide the UD's service cycle into the access process and the data transmission process. The five fixed slots are evenly divided into the data transmission process. We assume that all transmissions have the same priority in the contention-free scenario, and every UD and the AP always have packets to transmit in the optical link. The normalized average throughput of UD is a function of ς depicted in Fig. 8 with IHO, DHO and SHO methods. As illustrated, the normalized average throughput decreases with increasing ς for all scheme with the proposed method showing the lowest drop for $0.5 < \varsigma < 1.4\ \text{s}^{-1}$. Note that, for $\varsigma = 0.5\text{s}^{-1}$ and $1.4\ \text{s}^{-1}$, the proposed method offers higher throughputs of 26 and 11% compared with SHO, respectively.

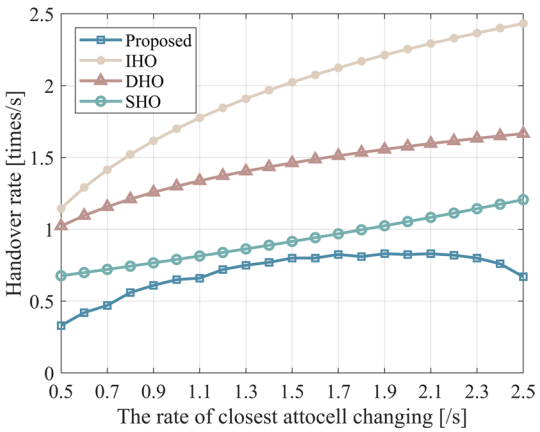

Fig. 7 Handover rate R_{ho} versus the rate of closest attocell changing. Figure illustrates the relationship of handover rate with the rate of closest attocell changing. Yellow, red, green and blue lines represent the manifestation of the immediate handover, the dwell handover, the handover skipping and we proposed handover scheme

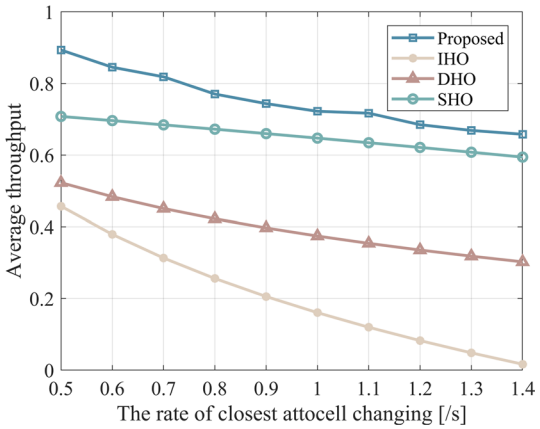

Fig. 8 The normalized average throughput of UD versus the rate of closest attocell changing. Figure illustrates the relationship of average throughput with the rate of closest attocell changing. Yellow, red, green and blue lines represent the manifestation of the immediate handover, the dwell handover, the handover skipping and we proposed handover scheme

6 Conclusion

This paper proposed a universal optical wireless terminal movement estimation and handover scheme based on uplink VLC channel in a bidirectional LiFi attocell experimental system, which could overcome the disadvantages of traditional approaches by using the uplink optical channel. The feasibility of the OWC handover scheme was compared with the other three approaches by simulation and experiment in the bidirectional VLC test-bed. Regarding the handover rate, the results showed that the proposed method could outperform IHO, DHO and SHO by 73%, 60% and 45%, respectively, and thus could be adapted in hybrid LiFi + 5G/6G (i.e., RF) and other OWC scenarios.

Abbreviations

LiFi	Light fidelity
OWC	Optical wireless communications
VLC	Visible light communications
IoT	Internet of things
IR	Infrared
AP	Access point
TDMA	Time division multiple access
RSRP	Reference signal received power
QoS	Quality of services
RF	Radio frequency
WiFi	Wireless fidelity
uRSRP	Uplink reference signal received power
UD	User device
RWP	Random waypoint
AM	Access mobility
FoV	Field of view
OA	Overlapping area
PD	Photodiode
FIFO	First-in-first-out
SNR	Signal-to-noise ratio
dRSRP	Downlink reference signal received power
PSD	Power spectral density
IHO	Immediate handover
DHO	Dwell handover
SHO	Skipping handover

Acknowledgements
Not applicable.

Author contributions
LW, DH and MZ proposed the dynamic handover scheme and designed the system model. JW and XJ implemented the simulation. LW analyzed results and drafted the manuscript. DH and JH revised the manuscript. All authors read and approved the final manuscript.

Funding
This research was supported by the National Natural Science Foundation of China (Grant No. 61675138) and the Fundamental Research Funds for the Central Universities (Grant No. 2019RC12).

Availability of data and materials
Not applicable.

Declarations

Competing interests
The authors declare that they have no competing interests.

Received: 13 June 2020 Accepted: 5 July 2022
Published online: 18 July 2022

References

1. T. Nguyen, D. Nguyen-Huu and T. Nguyen, On Achievable Rate Region Using Location Assisted Coding (LAC) for FSO Communication, In: *IEEE 86th Vehicular Technology Conference* (VTC-Fall, 2017), pp. 1–5
2. G. Zabih, W. Popoola , S. Rajbhandari, *Optical Wireless Communications : System and Channel Modelling with MATLAB* (Taylor & Francis, 2012)
3. A.C. Boucouvalas, P. Chatzimisios, Z. Ghassemlooy, M. Uysal, K. Yiannopoulos, Standards for indoor optical wireless communications. IEEE Commun. Mag. **53**(3), 24–31 (2015)
4. W. Ye, J. Chen, B. Lin, X. Tang, Z. Ghassemlooy, Experimental demonstration of bidirectional IDMA for visible light communication, In: 2017 *Opto-Electronics and Communications Conference* (OECC, 2017) *and Photonics Global Conference* (PGC 2017), pp. 1–3
5. M.B. Rahaim, T.D.C. Little, Toward practical integration of dual-use VLC within 5G networks. IEEE Wirel. Commun. **22**(4), 97–103 (2015)
6. Z. Ghassemlooy, L.N. Alves, S. Zvanovec, M. Alikhalighi, *Visible light communications: theory and applications* (Taylor & Francis, 2016)
7. F. Tariq, M. Khandaker, K.K. Wong, M. Imran, M. Bennis, M. Debbah, *A speculative study on 6G*, arXiv preprint arXiv:1902.06700 (2019)
8. X. Wu, H. Haas, Handover skipping for LiFi. IEEE. Access **7**, 38369–38378 (2019)
9. J.G. Andrews, S. Buzzi, W. Choi, S.V. Hanly, A. Lozano, A.C.K. Soong, J. Charlie Zhang, What will 5G be? IEEE J. Sel. Areas Commun. **32**(6), 1065–1082 (2014)
10. J. Hou, D.C. O'Brien, Vertical handover-decision-making algorithm using fuzzy logic for the integrated Radio-and-OW system. IEEE Trans. Wirel. Commun. **5**(1), 176–185 (2006)
11. E. Demarchou, C. Psomas, I. Krikidis, Mobility management in ultra-dense networks: handover skipping techniques. IEEE Access **6**, 11921–11930 (2018)
12. X. Ge, J. Ye, Y. Yang, Q. Li, User mobility evaluation for 5G small cell networks based on individual mobility model. IEEE J. Sel. Areas Commun. **34**(3), 528–541 (2016)
13. R. Arshad, H. ElSawy, S. Sorour, T. Y. Al-Naffouri, M-S. Alouini, Handover management in dense cellular networks: A stochastic geometry approach, In: *IEEE International Conference on Communications* (ICC, 2016), pp. 1–7
14. R. Arshad, H. Elsawy, S. Sorour, T.Y. Al-Naffouri, M.-S. Alouini, Handover management in 5G and beyond: a topology aware skipping approach. IEEE Access **4**, 9073–9081 (2016)
15. M. D. Soltani, X. Wu, M. Safari, H. Haas, Access point selection in Li-Fi cellular networks with arbitrary receiver orientation, In: *IEEE 27th Annual International Symposium on Personal, Indoor, and Mobile Radio Communications* (PIMRC, 2016), pp. 1–6
16. M. D. Soltani, H. Kazemi, M. Safari, H. Haas, Handover modeling for indoor Li-Fi cellular networks: The effects of receiver mobility and rotation, In: *IEEE Wireless Communications and Networking Conference* (WCNC, 2017), pp. 1–6
17. C. Le Bas, S. Sahuguede, A. Julien-Vergonjanne, A. Behlouli, P. Combeau, L. Aveneau, Impact of receiver orientation and position on visible light communication link performance, In: *4th International Workshop on Optical Wireless Communications* (IWOW, 2015), pp. 1–5
18. M.D. Soltani, A.A. Purwita, Z. Zeng, H. Haas, M. Safari, Modeling the random orientation of mobile devices: Measurement, analysis and LiFi use case. IEEE Trans. Commun. **67**(3), 2157–2172 (2018)
19. D. B. Johnson, D. A. Maltz, *Dynamic source routing in ad hoc wireless networks* (Mobile Computing, 1996)
20. A. K. Gupta, H. S. Dhillon, S. Vishwanath, J. G. Andrews, Downlink coverage probability in MIMO HetNets with flexible cell selection, In: *IEEE Global Communications Conference* (Globecom, 2014), pp. 1534–1539
21. A.C. Boucouvalas, P. Barker, Asymmetry in optical wireless links. IEEE Proc Optoelectron **147**(4), 315–321 (2000)
22. J.M. Kahn, J.R. Barry, Wireless infrared communications. Proc IEEE **85**(2), 265–298 (1997)
23. C. Hoymann, D. Larsson, H. Koorapaty, J.-F. Cheng, A lean carrier for LTE. IEEE Commun Mag **51**(2), 74–80 (2013)

Publisher's Note